

Partitioned active shape model with weighted landmarks for accurate lung field segmentation in pediatric chest radiography

Awais Mansoor¹, Geovanny F. Perez², Krishna Pancham², Abia Khan¹, Kazunori Okada³, Nino Gustavo², Marius G. Linguraru^{1,4}

¹Children's National Health System, Sheikh Zayed Institute for Pediatric Surgical Innovation, Washington DC, USA

²Children's National Health System, Pulmonology Department, Washington DC, USA

³San Francisco State University, Computer Science Department, San Francisco CA, USA

⁴George Washington University, School of Medicine and Health Sciences, Washington DC, USA

Keywords: active shape model (ASM), weighted landmarks, partitioned active shape model, local appearance model, chest radiographs, lung segmentation.

Purpose Despite tremendous advancements in tomographic imaging techniques, chest radiographs (CXR) remain the gold standard in pulmonary analysis mainly due to their low cost, low radiation dosage, and availability. Radiation dosage is of particular concern in pediatric applications [1]; accordingly, CXRs are still the preferred method of diagnosis in children. Therefore, there is a significant need for robust image analysis methods for pulmonary diagnosis that can yield clinical information from CXR thus avoiding high radiation dose associated with computed tomography images. Lung field segmentation is the necessary initial step for any pulmonary analysis and diagnosis. Accurate delineation of lung field from CXR is challenging due to ambiguous boundaries of lung field, existence of pathologies, superposition of non-target anatomical structures e.g., rib bones and heart, anatomical variation of lung shapes and size across subjects, and technical variations (rotation, expiratory phase), especially in children. There have been previous attempts in the literature for the segmentation of lung field from CXR; however, most attempts struggle to accommodate large anatomical and pathological variations found in pediatric CXRs. In addition, state-of-the-art existing methods, such as [2], do not delineate parts of lung field behind aortic arch and apex of heart in CXR (Fig. 1) and therefore annotate the lung field only partially. To address these shortcomings, we aim to develop a method for accurate lung field segmentation to accommodate the local anatomical and pathological variations that occur especially for pediatric CXRs with viral infections. Furthermore, the proposed method aims to accurately delineate the lung field areas behind aortic arch and apex of heart (blue regions in Fig.1 (b)).

Methods Study subjects. 30 posterior-anterior chest radiographs were collected at our institution from children between ages 0 to 2 years including individuals with acute viral respiratory infections, chronic lung conditions, chest wall deformities, cardiovascular anomalies and healthy controls. This study was approved by the Institutional Review Board at Children's National Health System. **Lung segmentation model.** We propose a weighted partitioned active shape model approach for the segmentation of lung fields. Traditional approaches of modeling the entire shape using one model are not optimal for structures with large shape and textural variability along their boundaries. In our proposed approach,

the lung field boundary is divided into several overlapping partitions to accommodate localized shape and appearance variations amongst subjects. Furthermore, the landmarks of training shapes are assigned weights according to their appearance confidence, thus using only reliable landmarks to deform the model. The method is divided into following main modules (Fig. 2(a)): **(1) Shape Initialization:** To infer initial lung shape, we adopt learning –based approach for landmark detection proposed in [2]; however, to increase robustness we also extract the ribcage as a contextual biomarker using a Hessian-based vessel enhancement filter. First, six manually annotated *primary* landmarks (shown in red in Fig. 2(b)) were obtained for each lung based on their distinctive anatomical appearance and ability to roughly define the shape of lung. Second, a feature set consisting of HOG and LBP [4] (31+58 features) are used in a cascade learning classifier for primary landmark detection. Finally, equidistant *secondary* landmarks (shown in green in Fig. 1(b)) are calculated along the lung contour using interpolation between the *primary* landmarks. **(2) Shape Sparse Learning:** To construct local partitions, the lung shape is divided into overlapping segments with consistent shape variations by performing soft-thresholding using fuzzy c-means clustering (Fig. 2(c)). The shape variation is determined based on the landmark position variation across training shapes and spatial distance. The optimal number of partitions is calculated based on the similarity matrix between position variation and spatial distance of landmarks. **(3) Appearance Sparse Learning:** A local appearance model consisting of three features is obtained to train local structure for each landmark: (i) normalized derivatives [3], (ii) tissue intensity probability (second class probability within three class fuzzy c-mean [3]), and (iii) elongated rib structure probability based on the vesselness filter (lungs are within the rib cage). Depending upon the image properties, presence of pathologies, and relevant discriminative information in the neighborhood, landmark locations may not be reliable; therefore, each landmark is assigned a weight based on a confidence metric. Landmarks with higher confidence weights have greater contribution in shape deformation. *Primary* landmarks are assigned the maximum confidence weight. For *secondary* landmarks the confidence weight is assigned based on local covariance of the normalized derivatives, tissue intensity probability, and vesselness. The reason for using the covariance matrix as confidence metric is that it encodes the local discriminative appearance of shape landmark. Lastly, the model fitting is performed individually for each partition and the optimal position of each landmark is determined by minimizing the Mahalanobis distance. The shape parameters of overlapping landmarks are calculated as mean shape parameters from the two overlapping partitions.

Results The CXRs for testing range from normal to having severe abnormalities including bibasilar opacities and diffuse infiltrates having dimensions 1607×1320 pixels with 0.143 mm/pixel and 16-bit gray levels. For evaluation and training purposes, the manual segmentation of radiographs was performed under the supervision of two board certified pulmonologists. We used leave-one-out cross-validation for evaluation purposes. Each lung in the CXR is divided into 6 partitions using inter- and intra-fuzzy cluster fluctuations of fuzzy c-means clustering. Experimental results show the accuracy and performance potential of the proposed approach over conventional ASM. We obtained an average overlap score (True Positive/(True Positive + False Positive+ False Negative)) of 0.9091 ± 0.068 compared to an overlap score of 0.8578 ± 0.608 for mean shape + ASM (p-value<0.001). In addition, Euclidean distance between landmark positions obtained using the proposed method and manually annotated ground-truth was 1.8821 ± 0.8612 mm (4.8381 ± 1.9126 mm for mean shape + ASM, p-value<0.001).

Conclusion We presented an accurate lung field segmentation method to overcome the challenge of large shape variations especially in pediatric subjects with large shape variations and lung pathologies. By using local appearance features, the proposed approach ensures that the areas behind aortic arch and apex of heart are included in the final segmentation. Future works includes individual co-segmentation of *red* and *blue* regions (Fig. 1) for accurate comparison with state-of-the-art methods, as well as textural learning based analysis to extract biomarkers of pulmonary infection severity using chest radiographs.

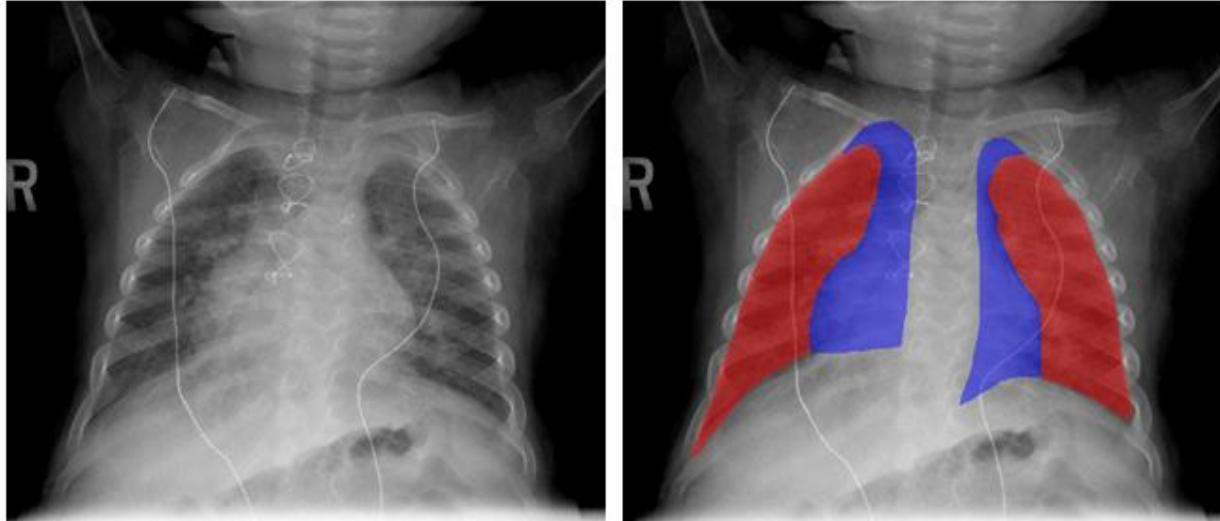
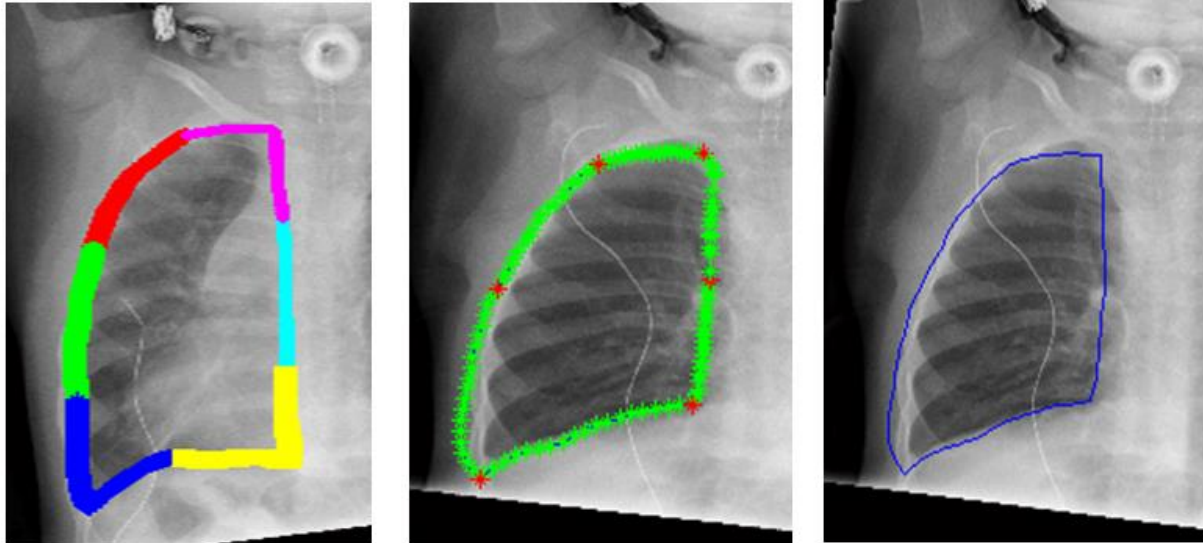


Fig. 1: (Left) A CXR image and **(Right)** the ground truth manual segmentation by an expert. The labels shown in blue are the regions of the lung field situated behind neighboring organs such as innominate veins, aortic arch and apex of heart.



(a)



(b)

(c)

(d)

Fig. 2: (a) The block diagram of the proposed method. (b) variation homogeneous shape partitioning of the lung boundary produced through FCM. (c) primary (red) and secondary (green) landmarks shown over the left lung of a pathologic case. (d) The segmented lung-field (blue) using the proposed method.

References

- [1] Diana L. Miglioretti, Eric Johnson, Andrew Williams, Robert T. Greenlee, Sheila Weinmann, Leif I. Solberg, Heather Spencer Feigelson, Douglas Roblin, Michael J. Flynn, Nicholas Vanneman, Rebecca Smith-Bindman, "The use of computed tomography in pediatrics and the associated radiation exposure and estimated cancer risk." *JAMA pediatrics* 167, no. 8 (2013): 700-707.
- [2] Yeqin Shao, Yaozong Gao, Yanrong Guo, Yonghong Shi, Xin Yang, Dinggang Shen, "Hierarchical Lung Field Segmentation With Joint Shape and Appearance Sparse Learning," *Medical Imaging, IEEE Transactions on*, vol.33, no.9, pp.1761,1780, Sept. 2014.
- [3] Xue Yang, Juan Cerrolaza, Chunzhe Duan, Qian Zhao, Jonathan Murnick, Nabile Safdar, Robert Avery, and Marius George Lingurar. "Weighted Partitioned Active Shape Model for Optic Pathway Segmentation in MRI." In *Clinical Image-Based Procedures. Translational Research in Medical Imaging*, pp. 109-117. Springer International Publishing, 2014.
- [4] Yun Fu, Liangliang Cao, Guodong Guo, and Thomas S. Huang. "Multiple feature fusion by subspace learning." In *Proceedings of the 2008 international conference on Content-based image and video retrieval*, pp. 127-134. ACM, 2008.